

---

# Tensor-Based Sketching Method for the Low-Rank Approximation of Data Streams

---

**Cuiyu Liu**  
Peking University  
2101213203@stu.pku.edu.cn

**Chuanfu Xiao**  
Peking University  
chuanfuxiao@pku.edu.cn

**Mingshuo Ding**  
Peking University  
dingmingshuo@pku.edu.cn

**Chao Yang**  
Peking University  
chao\_yang@pku.edu.cn

## Abstract

Low-rank approximation in data streams is a fundamental and significant task in computing science, machine learning and statistics. Multiple streaming algorithms have emerged over years and most of them are inspired by randomized algorithms, more specifically, sketching methods. However, many algorithms are not able to leverage information of data streams and consequently suffer from low accuracy. Existing data-driven methods improve accuracy but the training cost is expensive in practice. In this paper, from a subspace perspective, we propose a tensor-based sketching method for low-rank approximation of data streams. The proposed algorithm fully exploits the structure of data streams and obtains quasi-optimal sketching matrices by performing tensor decomposition on training data. A series of experiments are carried out and show that the proposed tensor-based method can be more accurate and much faster than the previous work.

## 1 Introduction

There are many scenarios that require batch or real-time processing of data streams arising from, e.g., video [6, 7], signal flow [3, 26], hyperspectral images [29, 32] and numerical simulations [31, 19]. A data stream can be seen as an ordered sequence of data continuously generated from one or several distributions [23, 14], and the data per time slot can be usually represented as a matrix. Therefore, most of the processing methods of data streams can be considered as operations on matrices, such as matrix multiplications, linear system solutions and low-rank approximation. Wherein, low-rank matrix approximation plays an important role in practical applications, such as independent component analysis (ICA) [27, 11], principle component analysis (PCA) [17, 16], image denoising [9, 32].

In this work, we consider low-rank approximation of matrices from a data stream. Specifically, let  $\{\mathbf{A}_d \in \mathbb{R}^{m \times n}\}_{d=1}^D$  be matrices from a data stream  $\mathcal{D}$ , then the low-rank approximation in  $\mathcal{D}$  can be described as:

$$\min_{\mathbf{B}} \|\mathbf{A}_d - \mathbf{B}\|_F, \quad \text{s.t. } \text{rank}(\mathbf{B}) \leq r, \quad (1.1)$$

where  $d = 1, 2, \dots, D$ ,  $\|\cdot\|_F$  represents the Frobenius norm, and  $r \in \mathbb{Z}_+$  is a user-specified target rank.

**Related work.** A direct approach to solve problem (1.1) is to calculate the truncated rank- $r$  singular value decomposition (SVD) of  $\mathbf{A}_d$  in turn, and the Eckart-Young theorem ensures that it is the best low-rank approximation [8]. However, it is too expensive to one by one calculate the truncated

rank- $r$  SVD of  $A_d$  for all  $d = 1, 2, \dots, D$ , particularly when  $m$  or  $n$  is large. To address this issue, many sketching algorithms have emerged such as the SCW algorithm [25, 4, 5]. Unfortunately, a notable weakness of sketching algorithms is that they achieve higher error than the best low-rank approximation, especially when the sketching matrix is generated randomly from some distribution, such as Gaussian, Cauchy, or Rademacher distribution [13, 30, 4, 10, 5]. To improve accuracy, a natural idea is to perform a preprocessing on the past data (seen as a training set) in order to better handle the future input matrices (seen as a test set). This approach, which is often called the data-driven approach, has gained more attention lately. For low-rank approximation, the pioneer of this work was [14], who proposed a learning-based method, that we henceforth refer to as IVY. In the IVY method, the sketching matrix is set to be sparse, and the values of non-zero entries are learned instead of setting them randomly as classical methods do. Specifically, learning is done by stochastic gradient descent (SGD), by optimizing a loss function that portrays the quality of the low-rank approximation obtained by the SCW algorithm as mentioned above. To improve accuracy, [22] followed the line of IVY by additionally optimizing the location of the non-zero entries of the sketching matrix  $S$ , not only their values. Recently, [15] proposed a Few-Shot data-driven low-rank approximation algorithm, and their motivation is to reduce the training time cost of [14]. Wherein, they proposed an algorithm namely FewShotSGD by minimizing a new loss function that measures the distance in subspace between the sketching matrix  $S$  and all left-SVD factor matrices of the training matrices, with SGD. However, these data-driven approaches all involve learning mechanisms, which require iterations during the optimization process. This raises a question: can we design an efficient method, such as a non-iterative method, to get a better sketching matrix with both short training time and high approximation quality? It would be an important step for the development of data-driven methods, especially in scenarios requiring low latency.

**Our contributions.** In this work, we propose a new data-driven approach for low-rank approximation of data streams, motivated by a subspace perspective. Specifically, we observe that a perfect sketching matrix  $S \in \mathbb{R}^{k \times m}$  should be close to the top- $k$  subspace of  $U^d$ , where  $U^d$  is the left-SVD factor matrix of  $A_d$ . Due to the relevance of matrices in a data stream, it allows us to develop a new sketching matrix  $S$  to approximate the top- $k$  subspace of  $U^d$  for all  $d = 1, \dots, D$ . Perhaps the heavy learning mechanisms can be eliminated. In fact, our approach attains the sketching matrix by minimizing a new loss function which is a relaxation of that in IVY. The most important thing is that we can get the minimization of this loss function by tensor decomposition on the training set, which is non-iterative. We refer to this method as tensor-based method. As an extension of the main approach, we also develop the two-sided tensor-based algorithm, which involves two sketching matrices  $S, W$ . These two sketching matrices can be obtained simultaneously by performing tensor decomposition once. Both algorithms are significantly faster and more accurate than the previous data-driven approaches.

## 2 Preliminaries

**The SCW algorithm.** Randomized SVD is an efficient algorithm for computing the low-rank approximation of matrices from a data stream. For example, the SCW algorithm, proposed by Sarlos, Clarkson and Woodruff [25, 4, 5], is a classical randomized SVD algorithm. The algorithm only computes the SVD of the compressed matrices  $SA$  and  $AV$ , and its time cost is  $\mathcal{O}(r^2(m+n))$  when we set  $k = \mathcal{O}(r)$ . The detailed procedure is shown in Algorithm 1.

---

**Algorithm 1** The SCW algorithm [25, 4, 5].

---

**Input:** Matrix  $A \in \mathbb{R}^{m \times n}$ , sketching matrix  $S \in \mathbb{R}^{k \times m}$ , and target rank  $r < \min\{m, n\}$

- 1:  $\tilde{A}, \tilde{V}, V^T \leftarrow$  full SVD of  $SA$
- 2:  $[AV]_r \leftarrow$  truncated rank- $r$  SVD of  $AV$
- 3:  $\hat{A} \leftarrow [AV]_r V^T$

**Output:** Low-rank approximation of  $A$ :  $\hat{A}$

---

In [4], it is proved that if  $S$  satisfies the property of Johnson-Lindenstrauss Lemma,  $k = \mathcal{O}(r \log(1/\delta)/\varepsilon)$  suffices the output  $\hat{A}$  to satisfy  $\|A - \hat{A}\|_F \leq (1 + \varepsilon)\|A - [A]_r\|_F$  with probability  $1 - \delta$ . Therefore, the approximation quality of the SCW algorithm is highly dependent on the choice

of the sketching matrix  $\mathbf{S}$ . In general, the randomly generated sketching matrix does not meet the accuracy requirements when we handle problems in a data stream, so can we design a new  $\mathbf{S}$  by utilizing the information of the data stream? This is the motivation of data-driven approaches.

**The IVY algorithm.** In [14], the sketching matrix  $\mathbf{S}$  is initialized by a sparse random sign matrix as described in [4]. The location of the non-zero entries is fixed, while the values are optimized with SGD via the loss function as follow.

$$\min_{\mathbf{S} \in \mathbb{R}^{k \times m}} \sum_{\mathbf{A} \in \mathcal{D}_{\text{train}}} \|\mathbf{A} - \text{SCW}(\mathbf{A}, \mathbf{S}, r)\|_F^2, \quad (2.1)$$

where  $\mathcal{D}_{\text{train}}$  is the training set sampled from the data stream  $\mathcal{D}$ . This requires computing the gradient of the SCW operator, which involves the SVD implementation (line 1 and 2 in Algorithm 1). IVY uses a differential but inexact SVD based on the power method, and [22] suggested that the SVD in PyTorch is also feasible and much more efficient.

**The Few-Shot algorithm.** In [15],  $\mathbf{S}$  is initialized the same way as IVY, and the location of non-zero entries remains, too. The difference is that the authors optimize the non-zero values by letting  $\mathbf{S}$  to approximate the left top- $r$  subspace of a few training matrices. Wherein, the proposed algorithm namely FewShotSGD minimizes the following loss function:

$$\min_{\mathbf{S} \in \mathbb{R}^{k \times m}} \sum_{\mathbf{U} \in \mathcal{U}_{\text{train}}} \|\mathbf{U}_r^T \mathbf{S}^T \mathbf{S} \mathbf{U} - \mathbf{I}_0\|_F^2, \quad (2.2)$$

where  $\mathcal{U}_{\text{train}} = \{\mathbf{U} : \mathbf{A} = \mathbf{U}\mathbf{\Sigma}\mathbf{V}^T \text{ of all } \mathbf{A} \in \mathcal{D}_{\text{train}}\}$ ,  $\mathbf{U}_r$  denotes a matrix containing the first  $r$  columns of  $\mathbf{U}$ , and  $\mathbf{I}_0 \in \mathbb{R}^{r \times n}$  has zero entries except that  $(\mathbf{I}_0)_{i,i} = 1$  for  $i = 1, \dots, r$ .

As shown in [15], the goal of FewShotSGD is to get the sketch which preserves the left top- $r$  subspace of all matrices  $\mathbf{A} \in \mathcal{D}_{\text{train}}$  well and meanwhile is orthogonal to their bottom- $(n-r)$  subspace. This raises a question: can we directly obtain a subspace that is close to the top- $r$  subspace of all  $\mathbf{A}$ s? The answer is yes! In this way, all matrices  $\mathbf{A} \in \mathcal{D}_{\text{train}}$  are required to be viewed as a whole, i.e., a third-order tensor. For illustration, we introduce some basics about tensor before presenting our method.

**Tensor basics.** For convenience, we only consider the third-order tensor  $\mathcal{A} \in \mathbb{R}^{m \times n \times D}$ , and  $\mathcal{A}_{i,j,d}$  represents the  $(i, j, d)$ -th entry of  $\mathcal{A}$ . The Frobenius norm of  $\mathcal{A}$  is defined as  $\|\mathcal{A}\|_F = \sqrt{\sum_{i,j,d} \mathcal{A}_{i,j,d}^2}$ .

The mode- $n$  ( $n = 1, 2, 3$ ) matricization of  $\mathcal{A}$  is to reshape it to a matrix  $\mathbf{A}_{(n)}$ . For example, the mode-1 matricization of  $\mathcal{A}$  is  $\mathbf{A}_{(1)} \in \mathbb{R}^{m \times nD}$  satisfying  $(\mathbf{A}_{(1)})_{i,1+(j-1)n+(d-1)mn} = \mathcal{A}_{i,j,d}$ . The 1-mode product of  $\mathcal{A}$  and a matrix  $\mathbf{S} \in \mathbb{R}^{k \times m}$  is denoted as  $\mathcal{B} = \mathcal{A} \times_1 \mathbf{S} \in \mathbb{R}^{k \times n \times D}$ , which satisfies  $\mathcal{B}_{s,j,d} = \sum_{i=1}^m \mathcal{A}_{i,j,d} \mathbf{S}_{s,i}$ . Tucker decomposition [28] is one format of tensor decomposition, which is also called higher-order singular value decomposition (HOSVD) [20]. It decomposes a tensor into a set of factor matrices and one small core tensor of the same order. For  $\mathcal{A} \in \mathbb{R}^{m \times n \times D}$ , its Tucker decomposition is

$$\mathcal{A} = \mathcal{G} \times_1 \mathbf{U} \times_2 \mathbf{V} \times_3 \mathbf{W},$$

where  $\mathbf{U} \in \mathbb{R}^{m \times r_1}$ ,  $\mathbf{V} \in \mathbb{R}^{n \times r_2}$ ,  $\mathbf{W} \in \mathbb{R}^{D \times r_3}$  are the column orthogonal factor matrices,  $\mathcal{G} \in \mathbb{R}^{r_1 \times r_2 \times r_3}$  is the core tensor, and  $(r_1, r_2, r_3)$  is called the multilinear-rank of  $\mathcal{A}$ . There are two important variations of Tucker decomposition, i.e., Tucker1 and Tucker2 [18] (1 or 2 modes of  $\mathcal{A}$  are decomposed), which can be represented as  $\mathcal{A} = \mathcal{G} \times_1 \mathbf{U}$  and  $\mathcal{A} = \mathcal{G} \times_1 \mathbf{U} \times_2 \mathbf{V}$ , respectively.

### 3 Tensor-based sketching method

In this section, we present our idea and method for low-rank approximation in data streams. The goal is to employ the given training set to get the sketch  $\mathbf{S}$ , inspired by IVY [14] and FewShotSGD [15].

#### 3.1 Tensor-based algorithm

Our main algorithm, the tensor-based algorithm, is also a data-driven algorithm for low-rank approximation in data streams. Instead of minimizing the loss (2.1) in IVY, we consider a different loss,

motivated by a subspace perspective. This loss function is easier to optimize than (2.1) since to get its minimization, only a Tucker1 decomposition is required, without learning mechanisms.

Let  $\mathcal{D}_{\text{train}} = \{\mathbf{A}_{d'} \in \mathbb{R}^{m \times n}\}_{d'=1}^{D'}$ , and the loss function we consider is

$$\min_{\mathbf{S} \in \mathbb{R}^{k \times m}} \sum_{\mathbf{A}_{d'} \in \mathcal{D}_{\text{train}}} \|\mathbf{A}_{d'} - \mathbf{S}^T \mathbf{S} \mathbf{A}_{d'}\|_F^2, \quad \text{s.t. } \mathbf{S} \mathbf{S}^T = \mathbf{I}_k. \quad (3.1)$$

Using the row-wise orthogonality of  $\mathbf{S}$ , we have  $\|\mathbf{A}_{d'} - \mathbf{S}^T \mathbf{S} \mathbf{A}_{d'}\|_F^2 = \|\mathbf{A}_{d'}\|_F^2 - \|\mathbf{S} \mathbf{A}_{d'}\|_F^2$ . Let  $\mathcal{A} \in \mathbb{R}^{m \times n \times D'}$  be a third-order tensor satisfying  $\mathcal{A}_{:, :, d'} = \mathbf{A}_{d'}$ . To minimize (3.1), it is equivalent to solve

$$\max_{\mathbf{S} \in \mathbb{R}^{k \times m}} \sum_{\mathbf{A}_{d'} \in \mathcal{D}_{\text{train}}} \|\mathbf{S} \mathbf{A}_{d'}\|_F^2 \iff \max_{\mathbf{S} \in \mathbb{R}^{k \times m}} \|\mathbf{S} \mathbf{A}_{(1)}\|_F^2, \quad \text{s.t. } \mathbf{S} \mathbf{S}^T = \mathbf{I}_k, \quad (3.2)$$

where  $\mathbf{A}_{(1)} = [\mathbf{A}_1 | \mathbf{A}_2 | \cdots | \mathbf{A}_{D'}]$  is the mode-1 matricization of  $\mathcal{A}$ . Further, as shown in [18], problem (3.2) is equivalent to

$$\begin{aligned} \min_{\mathbf{S} \in \mathbb{R}^{k \times m}} \|\mathcal{A} - \mathcal{G} \times_1 \mathbf{S}^T\|_F^2 \\ \text{s.t. } \mathcal{G} \in \mathbb{R}^{k \times n \times D'}, \quad \mathbf{S} \mathbf{S}^T = \mathbf{I}_k. \end{aligned} \quad (3.3)$$

This is a Tucker1 decomposition of  $\mathcal{A}$  along mode-1. Let  $\mathbf{A}_{(1)} = \mathbf{U}^{(1)} \mathbf{\Sigma}^{(1)} (\mathbf{V}^{(1)})^T$  be the SVD of  $\mathbf{A}_{(1)}$ . The optimal sketch  $\mathbf{S}^*$  for (3.3) is  $(\mathbf{U}^{(1)})_k^T$ , where  $(\mathbf{U}^{(1)})_k$  is a matrix composed of the first  $k$  columns in  $\mathbf{U}^{(1)}$  (refer to [18]). We use the optimal  $\mathbf{S}^*$  as input of SCW, and get the output of SCW as the low-rank approximation. The tensor-based algorithm is summarized in Algorithm 2.

The motivation behind this choice of loss function is the theorem below, which illustrates the relationship between our loss function (3.1) and that in IVY.

**Theorem 1.** *Let  $\mathbf{A}_{d'} \in \mathbb{R}^{m \times n}$  be a matrix from the training set, and  $\mathcal{A} \in \mathbb{R}^{m \times n \times D'}$  be a third-order tensor satisfying  $\mathcal{A}_{:, :, d'} = \mathbf{A}_{d'}$ . Given the target rank  $r \in \mathbb{Z}_+$ , and a row-wise orthogonal matrix  $\mathbf{S} \in \mathbb{R}^{k \times m}$ , for any positive integer  $k > r$ , we have*

$$\sum_{d'=1}^{D'} \|\mathbf{A}_{d'} - \text{SCW}(\mathbf{A}_{d'}, \mathbf{S}, r)\|_F^2 \leq \|\mathcal{A}\|_F^2 - \|[\mathbf{S} \mathbf{A}_{(1)}]_r\|_F^2, \quad (3.4)$$

where  $\mathbf{A}_{(1)} = [\mathbf{A}_1 | \mathbf{A}_2 | \cdots | \mathbf{A}_{D'}]$  is the mode-1 matricization of  $\mathcal{A}$ . Furthermore, with this relaxation, problem (2.1) can be converted to our proposed problem (3.3).

Theorem 1 justifies the rationality of our choice of the loss function. Below we give an analysis that using the sketch obtained by (3.3), the SCW computes a good low-rank approximation of  $\mathcal{A}$ .

**Analysis.** In fact, our idea is similar to that in [15] — both choosing the sketch  $\mathbf{S}$  to approximate the top- $r$  row subspace of matrices in  $\mathcal{D}_{\text{train}}$ . Let  $\mathbf{U} \mathbf{\Sigma} \mathbf{V}^T$  be the SVD of  $\mathcal{A}$ , where  $\mathbf{A}$  is a matrix in  $\mathcal{D}_{\text{train}}$ . Since there is strong relevance among matrices in  $\mathcal{D}_{\text{train}}$ , it makes sense to assume that  $\mathbf{S}$  obtained by (3.3) is close in space to  $\mathbf{U}_k$  ( $k > r$ ), where  $\mathbf{U}_k$  is a matrix composed of the first  $k$  columns of  $\mathbf{U}$ . In a special case where all matrices in  $\mathcal{D}_{\text{train}}$  are the same, i.e.,  $\mathbf{A}_{d'} = \mathbf{A}$  for  $d' = 1, \dots, D'$ , using  $\mathbf{S}$  obtained by (3.3), we have  $\|\mathbf{U}_k^T \mathbf{U}_k - \mathbf{S} \mathbf{S}^T\|_F^2 = 0$ . Theorem 2 shows that using  $\mathbf{S}$  computed by tensor-based algorithm, the SCW gives a good low-rank approximation of  $\mathcal{A}$  in a data stream.

**Theorem 2.** *Let  $\mathbf{U} \mathbf{\Sigma} \mathbf{V}^T$  be the SVD of  $\mathcal{A} \in \mathbb{R}^{m \times n}$ , and  $\mathbf{U}_k$  be a matrix composed of the first  $k$  columns of  $\mathbf{U}$ . Given a row-wise orthogonal sketching matrix  $\mathbf{S} \in \mathbb{R}^{k \times m}$  satisfying  $\|\mathbf{U}_k^T \mathbf{U}_k - \mathbf{S} \mathbf{S}^T\|_F^2 < \varepsilon$ , then we have*

$$\|\mathcal{A} - \text{SCW}(\mathcal{A}, \mathbf{S}, r)\|_F^2 - \|\mathcal{A} - [\mathcal{A}]_r\|_F^2 < \mathcal{O}(\varepsilon) \|\mathcal{A}\|_F^2. \quad (3.5)$$

The proofs of Theorem 1 and 2 are provided fully in the Appendix.

---

**Algorithm 2** The tensor-based algorithm for low-rank approximation of the data stream  $\mathcal{D}$ .

---

**Input:** Test matrix  $\mathbf{A}$ , training set  $\{\mathbf{A}_{d'} \in \mathbb{R}^{m \times n}\}_{d'=1}^{D'}$ , rank  $r \leq \min\{m, n\}$ , # rows of the sketching matrix  $k$ .

- 1: Tensorization:  $\mathcal{A} \in \mathbb{R}^{m \times n \times D'} \leftarrow \{\mathbf{A}_{d'}\}_{d'=1}^{D'}$
- 2:  $\mathbf{S} \leftarrow$  Tucker1 decomposition of  $\mathcal{A}$  along the mode-1
- 3:  $\hat{\mathbf{A}} \leftarrow \text{SCW}(\mathbf{A}, \mathbf{S}, r)$

**Output:** Low-rank approximation of  $\mathbf{A}$ :  $\hat{\mathbf{A}}$

---

### 3.2 Two-sided tensor-based algorithm

The two-sided tensor-based algorithm is an extension of the tensor-based algorithm in Section 3.1. The motivation is that if we compute the Tucker2 decomposition of  $\mathcal{A}$  mentioned in Theorem 1, two sketching matrices  $\mathbf{S}$  and  $\mathbf{W}$ , would be computed at once. This means that besides using  $\mathbf{S}$  for row space compression, we can use  $\mathbf{W}$  to compress the column space of  $\mathbf{A}$ , too. To be clear, we consider

$$\begin{aligned} \min_{\mathbf{S} \in \mathbb{R}^{k \times m}, \mathbf{W} \in \mathbb{R}^{l \times n}} \|\mathbf{A} - \mathcal{G} \times_1 \mathbf{S}^T \times_2 \mathbf{W}^T\|_F^2 \\ \text{s.t. } \mathcal{G} \in \mathbb{R}^{k \times l \times D'}, \\ \mathbf{S}\mathbf{S}^T = \mathbf{I}_k, \mathbf{W}\mathbf{W}^T = \mathbf{I}_l. \end{aligned} \quad (3.6)$$

Unlike (3.3), the exact solution of problem (3.6) has no explicit form, but can be efficiently approximated by an alternating iteration algorithm, namely higher-order orthogonal iteration (HOOI) [21, 18]. We present the HOOI algorithm in the Appendix. However, the SCW algorithm requires only one sketching matrix for computing low-rank approximation. As a result, a new sketching algorithm for two sketches is required.

**Two-sided SCW.** To this end, we develop a new algorithm for low-rank approximation based on the SCW algorithm, which we call two-sided SCW. It is worth mentioning that the full SVD in line 1 of Algorithm 1 is used for orthogonalization, thus it can be replaced with QR decomposition to improve the computational efficiency. With this in mind, the procedure of the two-sided SCW that we design is as shown in Algorithm 3.

---

**Algorithm 3** The two-sided SCW algorithm.

---

**Input:** Matrix  $\mathbf{A} \in \mathbb{R}^{m \times n}$ , sketching matrices  $\mathbf{S} \in \mathbb{R}^{k \times m}$  and  $\mathbf{W} \in \mathbb{R}^{l \times n}$ , and target rank  $r < \min\{m, n\}$

- 1:  $\mathbf{Q}, \sim \leftarrow$  QR decomposition of  $\mathbf{A}^T \mathbf{S}^T$
- 2:  $\mathbf{P}, \sim \leftarrow$  QR decomposition of  $\mathbf{A} \mathbf{W}^T$
- 3:  $[\mathbf{P}^T \mathbf{A} \mathbf{Q}]_r \leftarrow$  truncated rank- $r$  SVD of  $\mathbf{P}^T \mathbf{A} \mathbf{Q}$
- 4:  $\mathbf{P}[\mathbf{P}^T \mathbf{A} \mathbf{Q}]_r \mathbf{Q}^T \leftarrow$  low-rank approximation of  $\mathbf{A}$

**Output:** Low-rank approximation of  $\mathbf{A}$ :  $\hat{\mathbf{A}}$

---

Clearly, Algorithm 3 is more efficient than the original SCW when  $m, n$  are both large. The truncated SVD only needs to be done on  $\mathbf{P}^T \mathbf{A} \mathbf{Q} \in \mathbb{R}^{l \times k}$ , which is much smaller in size than  $\mathbf{A} \mathbf{V} \in \mathbb{R}^{m \times k}$  in Algorithm 1 ( $m > l$ ).

The procedure of the two-sided tensor-based algorithm is similar to the previously introduced tensor-based algorithm. First, reshape the training matrices to a third-order tensor  $\mathcal{A}$ . Then, obtain two sketching matrices  $\mathbf{S}, \mathbf{W}$  by computing the Tucker2 decomposition of  $\mathcal{A}$ . Finally, taking  $\mathbf{S}, \mathbf{W}$  and a test matrix  $\mathbf{A}$  as input, use two-sided SCW to get the low-rank approximation of  $\mathbf{A}$ . We summarize this in Algorithm 4. Recall that we compute the Tucker2 decomposition of  $\mathcal{A}$  by HOOI [21]. If  $k, l \sim \mathcal{O}(r)$ , the time cost for Tucker2 decomposition with HOOI is  $\mathcal{O}(r m n D' + r(m+n)D'^2)$ , while Tucker1 decomposition costs  $\mathcal{O}(m n^2 D')$ . In addition, as mentioned before, two-sided SCW is more efficient than the SCW algorithm. That means, the time complexity of the two-sided algorithm

is asymptotic less than the original tensor-based algorithm because  $r \ll m, n$ , usually. However, since two-sided SCW uses  $\mathbf{S}, \mathbf{W}$  to compress both the row and column space of  $\mathbf{A}$  while the SCW compresses the row space only, there would be some loss in accuracy for the two-sided tensor-based algorithm compared to the tensor-based one.

---

**Algorithm 4** The two-sided tensor-based algorithm for low-rank approximation of the data stream  $\mathcal{D}$ .

---

**Input:** Test matrix  $\mathbf{A}$ , training set  $\{\mathbf{A}_{d'} \in \mathbb{R}^{m \times n}\}_{d'=1}^{D'}$ , target rank  $r \leq \min\{m, n\}$ , # rows of the sketching matrix  $k$  and  $l$ .

- 1: Tensorization:  $\mathcal{A} \in \mathbb{R}^{m \times n \times D'} \leftarrow \{\mathbf{A}_{d'}\}_{d'=1}^{D'}$
- 2:  $\mathbf{S}, \mathbf{W} \leftarrow$  Tucker2 decomposition of  $\mathcal{A}$  along the mode-1 and 2
- 3:  $\hat{\mathbf{A}} \leftarrow$  Two-sided SCW( $\mathbf{A}, \mathbf{S}, \mathbf{W}, r$ )

**Output:** Low-rank approximation of  $\mathbf{A}$ :  $\hat{\mathbf{A}}$

---

## 4 Numerical experiments

In this section, we test our algorithms and compare them to the existing data-driven algorithms for low-rank approximation of data streams. We use three datasets for comparison — HSI [12], Logo [14] and MRI.

Table 1: Summary of datasets used for experiment.

Name	Description	Dimension	#Train	#Test
HSI <sup>1</sup>	Hyper spectral images	1024 × 768	100	400
Logo <sup>2</sup>	Video	3240 × 1920	100	400
MRI <sup>3</sup>	Magnetic resonance imaging	217 × 181	30	120

We measure the quality of the sketching matrix  $\mathbf{S}$  by the error on the test set, and the test error is defined as

$$\text{Error} = \frac{1}{|\mathcal{D}_{\text{test}}|} \sum_{\mathbf{A} \in \mathcal{D}_{\text{test}}} \frac{\|\mathbf{A} - \hat{\mathbf{A}}\|_F - \|\mathbf{A} - \mathbf{A}_{\text{opt}}\|_F}{\|\mathbf{A} - \mathbf{A}_{\text{opt}}\|_F}, \quad (4.1)$$

where  $\mathbf{A}_{\text{opt}}$  is the best rank- $r$  approximation of  $\mathbf{A}$ , and  $\hat{\mathbf{A}}$  is the low-rank approximation computed by the tested algorithms. In all experiments, we set the rank  $r$  to 10, and the sketching size  $k = l = 20$ . Experiments are run on a server equipped with an NVIDIA Tesla V100 card.

**Baselines.** As baselines, three methods are included — IVY [14], Few-Shot [15], and Butterfly [1].

*IVY.* As described in Ref. [14], the sketching matrix is initialized by a sign matrix. Its non-zero values are optimized by stochastic gradient descent (SGD) [24], which is an iterative optimization method widely used in machine learning.

*Few-Shot.* In [15], as IVY does, the sketching matrix is sparse, and the location of the non-zero entries is fixed. The non-zero values of the sketch are also optimized by SGD. They proposed one-shot closed-form algorithms (including *1Shot1Vec+IVY* and *1Shot2Vec*), and the FewShotSGD algorithm with either 2 or 3 randomly chosen training matrices (i.e., *FewShotSGD-2* and *FewShotSGD-3*). We compare our algorithms with all of them.

*Butterfly.* In [1], it is proposed to replace a dense linear layer in a neural network by the butterfly network. They suggested using a butterfly gadget for learning the low-rank approximation, also learning the non-zero values of a sparse sketching matrix by SGD, similarly to IVY.

<sup>1</sup>Retrieved from <https://github.com/gistairc/HS-SOD>.

<sup>2</sup>Retrieved from <http://youtu.be/L5HQoFIaT4I>.

<sup>3</sup>Retrieved from <https://brainweb.bic.mni.mcgill.ca/cgi/brainweb2>.

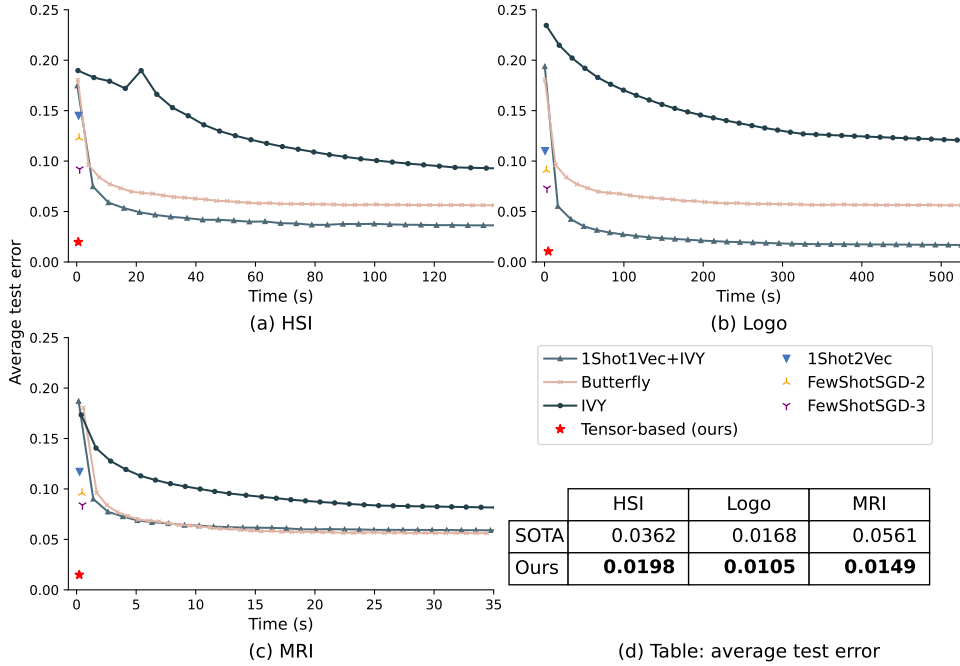


Figure 1: Test error per training time with the target rank  $r = 10$  and the sketching size  $k = 20$ . In (d), SOTA represents the lowest test error that the baselines achieve.

Since the baselines above all use one sketching matrix only, we compare our tensor-based algorithm with them. For the two-sided tensor-based algorithm, we test its performance later in this section, only comparing it with our tensor-based algorithm.

**Training time and test error.** We compare the test error per training time for each approach. The results are reported in Figure 1. The results show that our algorithm, the tensor-based algorithm, achieves the lowest error on all datasets. Table in (d) in Figure 1 lists the test error of the tensor-based algorithm and the lowest test error among the baselines. The tensor-based algorithm achieves at least **0.55/0.64/0.27** times lower test error on HSI/Logo/MRI than the baselines. On HSI/Logo/MRI, the tensor-based algorithm takes **0.53s/4.76s/0.23s** for training, which is much faster than *IVY*, *1Shot1Vec+IVY* and *Butterfly*. As a result, our algorithm significantly outperforms the baselines — much more accurate and faster.

Note that in the baselines, for better training, the training matrices have to be normalized to avoid the imbalance in the dataset. This requires computing the top singular values of the training matrices. On HSI/Logo/MRI, this normalization takes **46.55s/447.67s/0.72s**. The time for the normalization sometimes is even longer than the training time. We don't include this into the training time, but the pre-processing time. However, for the tensor-based algorithm and the two-sided tensor-based algorithm, this pre-processing time can be avoided, because our algorithms are to compute the top- $r$  subspace of the training matrices which remains when the training data scales by a constant.

**Testing time.** Next we report running time for the testing process on all datasets. Note that the sketching matrix by the tensor-based algorithm is dense, while that of the baselines is sparse. This results in the difference in the testing process, mainly on the matrix multiplication  $\mathbf{S}\mathbf{A}$  in the SCW procedure. The baselines have approximately the same testing time since their sketching matrix has the same sparsity. On HSI/Logo/MRI, the testing process for the tensor-based algorithm takes **0.52s/0.69s/0.28s**, while it takes **19.31s/60.15s/1.71s** for the baselines. The results seem unreasonable, because it is supposed to take more testing time with a dense sketching matrix. Actually, this is because for the tensor-based algorithm we use the built-in function in PyTorch (`torch.matmul( $\mathbf{S}$ ,  $\mathbf{A}$ )`) to compute  $\mathbf{S}\mathbf{A}$ . However, for the baselines, the sketching matrix  $\mathbf{S}$  is sparse and  $\mathbf{S}$  is stored using two vectors — one for storing the location of non-zero entries, and another for storing the values of the non-zero entries. We have no idea how to accelerate the matrix multiplication  $\mathbf{S}\mathbf{A}$  while exploiting the sparse structure of  $\mathbf{S}$ . Note that we surely can store the sparse  $\mathbf{S}$  in the

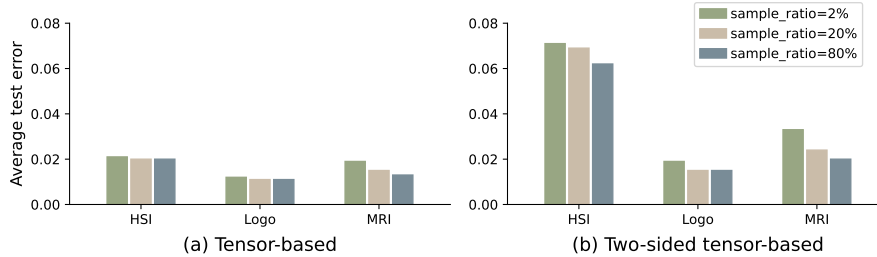


Figure 2: Test error of the tensor-based algorithm and the two-sided tensor-based algorithm under different number of training samples.

dense form and also apply  $\text{torch.matmul}(\mathbf{S}, \mathbf{A})$  to compute  $\mathbf{SA}$ . But then the sparsity of  $\mathbf{S}$  does not provide any advantage either.

**Experiments for the two-sided algorithm.** Finally, we test the performance of the two-sided tensor-based algorithm. This algorithm uses two sketching matrices  $\mathbf{S}, \mathbf{W}$  for computing the low-rank approximation. Table 2 shows the test error, the training time and the testing time for the two proposed algorithms, the tensor-based algorithm and two-sided version. The tensor-based algorithm achieves **0.29/0.73/0.63** times lower test error on HSI/Logo/MRI than the two-sided algorithm. However, the two-sided algorithm has both shorter training time and testing time. These results confirm our analysis in Section 3.

Table 2: Test error, training time and testing time of the tensor-based algorithm and the two-sided tensor-based algorithm.

Datasets	Algorithms	test error	training time (s)	testing time (s)
HSI	tensor-based	0.020	0.53	0.52
	two-sided	0.069	0.39	0.41
Logo	tensor-based	0.011	4.76	0.69
	two-sided	0.015	1.36	0.50
MRI	tensor-based	0.015	0.23	0.28
	two-sided	0.024	0.17	0.12

**Additional experiments.** In the experiments above, we only evaluate the algorithms when the sample ratio for training is 20% ( $\frac{100}{100+400} = \frac{100}{100+400} = \frac{30}{30+120} = 20\%$  for HSI/Logo/MRI, respectively), which we denote as  $\text{sample\_ratio} = 20\%$ . Figure 2 shows the performance of our proposed algorithms under different values of  $\text{sample\_ratio}$ , including 2%, 20% and 80%. The results show that using only a small number of training matrices ( $\text{sample\_ratio} = 2\%$  for example), our algorithms achieve low enough error. When  $\text{sample\_ratio}$  increases from 2% to 80%, the test error of the tensor-based algorithm decreases by a multiplicative factor of **0.952/0.917/0.684** on HSI/Logo/MRI, and for the two-sided tensor-based algorithm, the corresponding factor is **0.873/0.789/0.606** on HSI/Logo/MRI. On MRI, the test error decreases more when the number of training matrices increases compared to the other two datasets. In our opinion, this is because there is less stronger relevance among matrices of MRI. In general, increasing training samples improves the accuracy, but not significantly.

For our approach, one of the limitations is that it is required to load the whole training tensor at once. But for the baselines, the sketching matrix is learned by SGD and one of its advantages is that only a few (batch-size) training matrices are required to load in memory at a time. However, the results in Figure 2 show that a small number of training matrices are enough to achieve good low-rank approximation for both the tensor-based algorithm and the two-sided tensor-based algorithm. As a result, the memory usage of the proposed algorithms is also relatively low, comparable to the baselines.



## 5 Conclusions and future work

In this work, we propose an efficient and accurate approach to deal with low-rank approximation of data streams, namely the tensor-based sketching method. From a subspace perspective, we develop a tensor-based algorithm as well as a two-sided tensor-based algorithm. Numerical experiments show that the two-sided tensor-based algorithm is faster but attains higher test error than the tensor-based algorithm. Compared to the baselines, both algorithms are not only more accurate, but also far more efficient.

This work mainly focuses on reducing the training time for generating the sketching matrix. However, reducing the testing time is also of great interest. One of the approaches is to develop pass-efficient sketching-based algorithms for low-rank approximation. In applications, the pass-efficiency becomes crucial when the data size exceeds memory available in RAM. Further, in addition to low-rank approximation, the idea of the tensor-based sketching method can be applied to more operations such as  $\varepsilon$ -approximation and linear system solutions on data streams. We leave them for future work.

## References

- [1] N. Ailon, O. Leibovitch, and V. Nair. Sparse linear networks with a fixed butterfly structure: theory and practice. In *Uncertainty in Artificial Intelligence*, pages 1174–1184. PMLR, 2021.
- [2] D. Carlson. Minimax and interlacing theorems for matrices. *Linear Algebra and its Applications*, 54:153–172, 1983.
- [3] A. Cichocki, D. Mandic, L. De Lathauwer, G. Zhou, Q. Zhao, C. Caiafa, and H. A. Phan. Tensor decompositions for signal processing applications: From two-way to multiway component analysis. *IEEE Signal Processing Magazine*, 32(2):145–163, 2015.
- [4] K. L. Clarkson and D. P. Woodruff. Numerical linear algebra in the streaming model. In *Proceedings of the forty-first annual ACM symposium on Theory of computing*, pages 205–214, 2009.
- [5] K. L. Clarkson and D. P. Woodruff. Low-rank approximation and regression in input sparsity time. *Journal of the ACM (JACM)*, 63(6):1–45, 2017.
- [6] B. Cyganek and M. Woźniak. Tensor-based shot boundary detection in video streams. *New Generation Computing*, 35(4):311–340, 2017.
- [7] S. Das. Hyperspectral image, video compression using sparse Tucker tensor decomposition. *IET Image Processing*, 15(4):964–973, 2021.
- [8] C. Eckart and G. Young. The approximation of one matrix by another of lower rank. *Psychometrika*, 1(3):211–218, 1936.
- [9] Q. Guo, C. Zhang, Y. Zhang, and H. Liu. An efficient SVD-based method for image denoising. *IEEE Transactions on Circuits and Systems for Video Technology*, 26(5):868–880, 2015.
- [10] N. Halko, P. G. Martinsson, and J. A. Tropp. Finding structure with randomness: Probabilistic algorithms for constructing approximate matrix decompositions. *SIAM Review*, 53(2):217–288, 2011.
- [11] A. Hyvärinen. Independent component analysis: Recent advances. *Philosophical Transactions of the Royal Society A: Mathematical, Physical and Engineering Sciences*, 371(1984):20110534, 2013.
- [12] N. Imamoglu, Y. Oishi, X. Zhang, G. Ding, Y. Fang, T. Kouyama, and R. Nakamura. Hyperspectral image dataset for benchmarking on salient object detection. In *2018 Tenth International Conference on Quality of Multimedia Experience (qoMEX)*, pages 1–3. IEEE, 2018.
- [13] P. Indyk. Stable distributions, pseudorandom generators, embeddings, and data stream computation. *Journal of the ACM (JACM)*, 53(3):307–323, 2006.
- [14] P. Indyk, A. Vakilian, and Y. Yuan. Learning-based low-rank approximations. In *Proceedings of the 33rd International Conference on Neural Information Processing Systems*, pages 7402–7412, 2019.
- [15] P. Indyk, T. Wagner, and D. P. Woodruff. Few-shot data-driven algorithms for low rank approximation. *Advances in Neural Information Processing Systems*, 34:10678–10690, 2021.

- [16] I. T. Jolliffe and J. Cadima. Principal component analysis: A review and recent developments. *Philosophical Transactions of the Royal Society A: Mathematical, Physical and Engineering Sciences*, 374(2065):20150202, 2016.
- [17] S. Karamizadeh, S. M. Abdullah, A. A. Manaf, M. Zamani, and A. Hooman. An overview of principal component analysis. *Journal of Signal and Information Processing*, 4, 2020.
- [18] T. G. Kolda and B. W. Bader. Tensor decompositions and applications. *SIAM Rev.*, 51(3):455–500, 2009.
- [19] T. Von Larcher and R. Klein. Approximating turbulent and non-turbulent events with the tensor train decomposition method. In *Turbulent Cascades II*, pages 283–291. Springer, 2019.
- [20] L. De Lathauwer, B. De Moor, and J. Vandewalle. A multilinear singular value decomposition. *SIAM J. Matrix Anal. Appl.*, 21(4):1253–1278, 2000.
- [21] L. De Lathauwer, B. De Moor, and J. Vandewalle. On the best rank-1 and rank- $(R_1, R_2, \dots, R_N)$  approximation of higher-order tensors. *SIAM J. Matrix Anal. Appl.*, 21:1324–1342, 2000.
- [22] S. Liu, T. Liu, A. Vakilian, Y. Wan, and D. P. Woodruff. Learning the positions in counts sketch. *arXiv preprint arXiv:2007.09890*, 2020.
- [23] S. Muthukrishnan. *Data streams: Algorithms and applications*. Now Publishers Inc, 2005.
- [24] D. Saad. Online algorithms and stochastic approximations. *Online Learning*, 5:6–3, 1998.
- [25] R. Sarlos. Improved approximation algorithms for large matrices via random projections. In *2006 47th Annual IEEE Symposium on Foundations of Computer Science (FOCS'06)*, pages 143–152. IEEE, 2006.
- [26] N. D. Sidiropoulos, L. De Lathauwer, X. Fu, K. Huang, E. E. Papalexakis, and C. Faloutsos. Tensor decomposition for signal processing and machine learning. *IEEE Transactions on Signal Processing*, 65(13):3551–3582, 2017.
- [27] J. V. Stone. Independent component analysis: An introduction. *Trends in cognitive sciences*, 6(2):59–64, 2002.
- [28] L. R. Tucker. Some mathematical notes on three-mode factor analysis. *Psychometrika*, 31:279–311, 1966.
- [29] Y. Wang, J. Peng, Q. Zhao, Y. Leung, X. Zhao, and D. Meng. Hyperspectral image restoration via total variation regularized low-rank tensor decomposition. *IEEE Journal of Selected Topics in Applied Earth Observations and Remote Sensing*, 11(4):1227–1243, 2017.
- [30] F. Woolfe, E. Liberty, V. Rokhlin, and M. Tygert. A fast randomized algorithm for the approximation of matrices. *Applied and Computational Harmonic Analysis*, 25(3):335–366, 2008.
- [31] G. Zhang, X. Zheng, S. Liu, M. Chen, C. Wang, and X. Wang. Three-dimensional wind velocity reconstruction based on tensor decomposition and CFD data with experimental verification. *Energy Conversion and Management*, 256:115322, 2022.
- [32] H. Zhang, L. Liu, W. He, and L. Zhang. Hyperspectral image denoising with total variation regularization and nonlocal low-rank tensor decomposition. *IEEE Transactions on Geoscience and Remote Sensing*, 58(5):3071–3084, 2019.

## A Appendix

### A.1 Proof of Theorem 1

**Proof.** The inequality in (3.4) will be proved if we prove the following two inequalities.

$$\sum_{d'=1}^{D'} \|\mathbf{A}_{d'} - \text{SCW}(\mathbf{S}, \mathbf{A}_{d'})\|_F^2 \leq \sum_{d'=1}^{D'} \|\mathbf{A}_{d'} - \mathbf{S}^T[\mathbf{S}\mathbf{A}_{d'}]_r\|_F^2, \quad (\text{A.1})$$

and

$$\sum_{d'=1}^{D'} \|\mathbf{A}_{d'} - \mathbf{S}^T[\mathbf{S}\mathbf{A}_{d'}]_r\|_F^2 \leq \|\mathcal{A}\|_F^2 - \|[\mathbf{S}\mathbf{A}_{(1)}]_r\|_F^2. \quad (\text{A.2})$$

First, we consider the inequality in (A.1). Let  $\mathbf{Q} \in \mathbb{R}^{n \times k}$  be a column-wise orthogonal matrix in the row space of  $\mathbf{S}\mathbf{A}_{d'}$ . By definition of SCW, we have

$$\|\mathbf{A}_{d'} - \text{SCW}(\mathbf{S}, \mathbf{A}_{d'})\|_F^2 = \|\mathbf{A}_{d'} - [\mathbf{A}_{d'}\mathbf{Q}]_r\mathbf{Q}^T\|_F^2 = \|\mathbf{A}_{d'}\|_F^2 - \|[\mathbf{A}_{d'}\mathbf{Q}]_r\|_F^2. \quad (\text{A.3})$$

Similarly,

$$\|\mathbf{A}_{d'} - \mathbf{S}^T[\mathbf{S}\mathbf{A}_{d'}]_r\|_F^2 = \|\mathbf{A}_{d'}\|_F^2 - \|[\mathbf{S}\mathbf{A}_{d'}]_r\|_F^2. \quad (\text{A.4})$$

Combing (A.3) and (A.4), (A.1) follows immediately if we show

$$\|[\mathbf{S}\mathbf{A}_{d'}]_r\|_F \leq \|[\mathbf{A}_{d'}\mathbf{Q}]_r\|_F. \quad (\text{A.5})$$

Noting that

$$\mathbf{S}\mathbf{A}_{d'}\mathbf{Q} = \mathbf{U}\Sigma\mathbf{V}^T\mathbf{Q} = \mathbf{U}\Sigma\mathbf{Q}',$$

where  $\mathbf{U}\Sigma\mathbf{V}^T$  is the singular value decomposition of  $\mathbf{S}\mathbf{A}_{d'}$  and  $\mathbf{Q}' = \mathbf{V}^T\mathbf{Q}$ . Since  $\mathbf{V}$  and  $\mathbf{Q}$  lie in the same row space and are both column-wise orthogonal, it is easy to see that  $\mathbf{Q}'$  is a  $k$ -dimensional orthogonal matrix. Thus,  $\mathbf{S}\mathbf{A}_{d'}$  and  $\mathbf{S}\mathbf{A}_{d'}\mathbf{Q}$  share the same singular values. Combining Cauchy interlace theorem [2], we have

$$\|[\mathbf{S}\mathbf{A}_{d'}]_r\|_F = \|[\mathbf{S}\mathbf{A}_{d'}\mathbf{Q}]_r\|_F \leq \|[\mathbf{A}_{d'}\mathbf{Q}]_r\|_F, \quad (\text{A.6})$$

which proves (A.5).

We now turn to the inequality in (A.2). For convenience, we rewritten  $\mathbf{S}\mathbf{A}_{(1)}$  and  $[\mathbf{S}\mathbf{A}_{(1)}]_r$  with block components as

$$\mathbf{S}\mathbf{A}_{(1)} = [\mathbf{S}\mathbf{A}_1 | \mathbf{S}\mathbf{A}_2 | \cdots | \mathbf{S}\mathbf{A}_{D'}],$$

and

$$[\mathbf{S}\mathbf{A}_{(1)}]_r = [\mathbf{B}_1 | \mathbf{B}_2 | \cdots | \mathbf{B}_{D'}],$$

where  $\mathbf{B}_i \in \mathbb{R}^{k \times n}$  for  $i = 1, \dots, D'$ . We then have

$$\begin{aligned} \sum_{d'=1}^{D'} \|\mathbf{S}\mathbf{A}_{d'}\|_F^2 - \sum_{d'=1}^{D'} \|[\mathbf{S}\mathbf{A}_{d'}]_r\|_F^2 &= \sum_{d'=1}^{D'} \|\mathbf{S}\mathbf{A}_{d'} - [\mathbf{S}\mathbf{A}_{d'}]_r\|_F^2 \\ &\leq \sum_{d'=1}^{D'} \|\mathbf{S}\mathbf{A}_{d'} - \mathbf{B}_{d'}\|_F^2 \\ &= \|\mathbf{S}\mathbf{A}_{(1)}\|_F^2 - \|[\mathbf{S}\mathbf{A}_{(1)}]_r\|_F^2, \end{aligned}$$

where the Eckart-Young theorem is applied. It follows that

$$\sum_{d'=1}^{D'} \|[\mathbf{S}\mathbf{A}_{d'}]_r\|_F^2 \geq \|[\mathbf{S}\mathbf{A}_{(1)}]_r\|_F^2,$$

which is equivalent to in (A.2).

Hence, we have proved that  $\|\mathbf{A}\|_F^2 - \|[\mathbf{S}\mathbf{A}_{(1)}]_r\|_F^2$  is a relaxation of  $\sum_{\mathbf{A}_{d'} \in \mathcal{D}_{\text{train}}} \|\mathbf{A}_{d'} - \text{SCW}(\mathbf{S}, \mathbf{A}_{d'})\|_F^2$ . Therefore, the problem (2.1) can be converted to minimize  $\|\mathbf{A}\|_F^2 - \|[\mathbf{S}\mathbf{A}_{(1)}]_r\|_F^2$ , i.e., maximize  $\|[\mathbf{S}\mathbf{A}_{(1)}]_r\|_F^2$ . Due to  $k > r$ , it is not difficult to verify that a sufficient condition for maximizing  $\|[\mathbf{S}\mathbf{A}_{(1)}]_r\|_F^2$  is maximizing  $\|\mathbf{S}\mathbf{A}_{(1)}\|_F^2$ , which is equivalent to (3.3). As a result, instead of optimizing problem (2.1), we can convert it to our proposed problem (3.3).

Hence, our proof is completed.  $\square$

## A.2 Proof of Theorem 2

**Proof.** Let  $\hat{\mathbf{U}}\hat{\Sigma}\hat{\mathbf{V}}^T$  be the SVD of the matrix  $\mathbf{S}\mathbf{A}$ . Using the definition of the SCW algorithm, we have  $\text{SCW}(\mathbf{A}, \mathbf{S}, r) = [\mathbf{A}\hat{\mathbf{V}}]_r\hat{\mathbf{V}}^T$ . Further, since  $\hat{\mathbf{V}}$  is column-wise orthogonal, we have

$$\|\mathbf{A} - \text{SCW}(\mathbf{A}, \mathbf{S}, r)\|_F^2 = \|\mathbf{A} - [\mathbf{A}\hat{\mathbf{V}}]_r\hat{\mathbf{V}}^T\|_F^2 = \|\mathbf{A}\|_F^2 - \|[\mathbf{A}\hat{\mathbf{V}}]_r\|_F^2.$$

Similarly, we have

$$\|\mathbf{A} - [\mathbf{A}]_r\|_F^2 = \|\mathbf{A}\|_F^2 - \|[\mathbf{U}_k^T \mathbf{A}]_r\|_F^2.$$

Recall that  $U\Sigma V^T$  is the SVD of  $\mathbf{A}$ , and  $U_k$  be a matrix composed of the first  $k$  columns of  $U$ . Based on the result (A.6) in the proof of Theorem 1, we immediately get

$$\|[\mathbf{A}\hat{\mathbf{V}}]_r\|_F^2 \geq \|[\mathbf{S}\mathbf{A}]_r\|_F^2. \quad (\text{A.7})$$

Thus, we have

$$\begin{aligned} \|\mathbf{A} - \text{SCW}(\mathbf{A}, \mathbf{S}, r)\|_F^2 - \|\mathbf{A} - [\mathbf{A}]_r\|_F^2 &\leq \|[\mathbf{U}_k^T \mathbf{A}]_r\|_F^2 - \|[\mathbf{S}\mathbf{A}]_r\|_F^2 \\ &\leq \|\mathbf{U}_k^T \mathbf{A}\|_F^2 - \|\mathbf{S}\mathbf{A}\|_F^2 \\ &= \text{tr}(\mathbf{A}^T (\mathbf{U}_k \mathbf{U}_k^T - \mathbf{S}^T \mathbf{S}) \mathbf{A}) \\ &\leq \|\mathbf{U}_k \mathbf{U}_k^T - \mathbf{S}^T \mathbf{S}\|_2^2 \|\mathbf{A}\|_F^2 \\ &\leq \|\mathbf{U}_k \mathbf{U}_k^T - \mathbf{S}^T \mathbf{S}\|_F^2 \|\mathbf{A}\|_F^2 \\ &\leq \mathcal{O}(\varepsilon) \|\mathbf{A}\|_F^2. \end{aligned} \quad (\text{A.8})$$

Hence, our proof is completed.  $\square$

### A.3 HOOI algorithm

---

**Algorithm 5** HOOI algorithm [21, 18]

---

**Input:**

Tensor  $\mathcal{A} \in \mathbb{R}^{I_1 \times I_2 \times \dots \times I_N}$

Truncation  $(R_1, R_2, \dots, R_N)$

Initial guess  $\{\mathbf{U}_0^{(n)} : n = 1, 2, \dots, N\}$

**Output:**

Low multilinear-rank approximation  $\hat{\mathcal{A}} = \mathcal{G} \times_1 \mathbf{U}^{(1)} \times_2 \mathbf{U}^{(2)} \dots \times_N \mathbf{U}^{(N)}$

1:  $k \leftarrow 0$

2: **while** not convergent **do**

3:   **for all**  $n \in \{1, 2, \dots, N\}$  **do**

4:      $\mathcal{B} \leftarrow \mathcal{A} \times_1 (\mathbf{U}_{k+1}^{(1)})^T \dots \times_{n-1} (\mathbf{U}_{k+1}^{(n-1)})^T \times_{n+1} (\mathbf{U}_k^{(n+1)})^T \dots \times_N (\mathbf{U}_k^{(N)})^T$

5:      $\mathbf{B}_{(n)} \leftarrow \mathcal{B}$  in matrix format

6:      $\mathbf{U}, \Sigma, \mathbf{V}^T \leftarrow$  truncated rank- $R_n$  SVD of  $\mathbf{B}_{(n)}$

7:      $\mathbf{U}_{k+1}^{(n)} \leftarrow \mathbf{U}$

8:      $\mathcal{G}_{k,n} \leftarrow \Sigma \mathbf{V}^T$  in tensor format

9:      $k \leftarrow k + 1$

10:   **end for**

11: **end while**

12:  $\mathcal{G} \leftarrow \Sigma \mathbf{V}^T$  in tensor format

---